Bose-Einstein condensate immersed in a Fermi sea: Theory of static and dynamic behavior across phase separation

Bo Huang (黄博) [*]

Institut für Quantenoptik und Quanteninformation (IQOQI), Österreichische Akademie der Wissenschaften, 6020 Innsbruck, Austria
and Institut für Experimentalphysik und Zentrum für Quantenphysik, Universität Innsbruck, 6020 Innsbruck, Austria

We theoretically study the static and dynamic behavior of a BEC immersed in a large Fermi sea of ultracold atoms under conditions of tunable interspecies interaction. The degenerate Bose-Fermi mixture is kept in an elongated trap, typical for a single-beam optical dipole trap. We focus on the case of repulsive Bose-Fermi interaction and develop mean-field models to simulate the system over a wide range of repulsion strength. We further get analytical solutions in the regimes of phase separation and weak interaction. We obtain static density profiles and the frequency of the radial breathing mode, which is an elementary dynamic phenomenon of the mixture. Our results unveil the structure of the Bose-Fermi interface and describe the origin of the frequency shift of the breathing mode when the components become phase-separated at strong repulsion. We show that the mediated interaction between bosons induced by the Fermi sea can be understood as an adiabatic second-order mean-field effect, which is valid also beyond the weak-interaction regime for relevant experimental conditions. These results are consistent with our recent observations [Lous *et al.*, Phys. Rev. Lett. **120**, 243403 (2018); Huang *et al.*, Phys. Rev. A **99**, 041602(R) (2019)] in a mixture of ^{41}K and ^{6}Li.

I. INTRODUCTION

Historically, studies on multicomponent quantum fluids have been conducted on mixtures of ^{3}He with ^{4}He [1] and hydrogen with deuterium or tritium [2]. The more recent achievements with ultracold atomic gases [3,4], in which the interatomic interactions can be tuned by Feshbach resonances [5], offer experimentalists many opportunities to create and study interacting quantum mixtures of different spin states, isotopes, or species. One situation is mixing quantum fluids of different quantum statistics: degenerate Fermi gases (DFGs) and Bose-Einstein condensates (BECs) [6,7]. In these mixtures, interspecies interactions between fermions and superfluid BECs lead to rich phase diagrams (e.g., [8]) and dynamic phenomena [9].

The equilibrium state of degenerate Bose-Fermi mixtures and their stability have been studied in experiments [10,11,26] and also in mean-field theories, in which often the zero-temperature case is considered [12,13]. It is a well-established fact that the constituents of a mixture undergo phase separation when the interaction is repulsive and strong, and the BEC collapses when the interaction is substantially attractive. An important phenomenon of phase separation is the formation of a thin interface between the components, and the remaining boson-fermion overlap at the interface has recently been probed by measuring three-body recombination losses in a ^{41}K-^{6}Li mixture [26]. Therefore we are encouraged to investigate the detailed structure and properties of the thin interface theoretically.

Generally, collective excitations of the BEC can be described by the Gross-Pitaevskii equation (GPE) [4], and the evolution of the DFG is analyzed either with kinetic equations in a semiclassical manner or via response functions of perturbations [14,15]. The latter are rather different from superfluid fermions [9], which can be described by order parameter and hydrodynamic equations. In a miscible mixture, interspecies interaction is modeled as a mean field to study elementary excitations of zero-temperature Bose-Fermi mixtures under homogeneous [16] and harmonically trapped [17] conditions. In the limit of full phase separation, the BEC and DFG establish a pressure balance at the interface, and their collective modes in a harmonic trap have been investigated [18,19]. There also have been efforts to understand the dynamics over a range of interaction strengths, and a numerical model for the time evolution of monopole oscillations in a Bose-Fermi mixture has been constructed in Ref. [20].

Recent experiments have studied the center-of-mass (COM) mode of a BEC coupled to either a fermionic superfluid [21–24] or a DFG [25]. The interspecies interaction is weak in the first case while being tunable in the latter. In both cases, very small frequency shifts, of the order of a few percent, have been observed. However, our recent measurements on the radial breathing mode (RBM) frequency demonstrate a striking frequency shift of up to about 40% at phase separation [26,27], whereas the frequency remains almost unchanged when bosons and fermions are mixed.

In this work, we elaborate a set of mean-field models used in Refs. [26,27] and present novel explanations of the structure of the Bose-Fermi interface and the mediated

---

*bo.huang@uibk.ac.at

boson-boson interaction. We consider the situation in our recent experiments [26,27]. A small BEC is immersed in a large Fermi sea and both components are trapped in an elongated harmonic trap. We first set up a mean-field model and numerically calculate the static density profiles of the Bose-Fermi mixture at zero temperature and extract the overlap between the two components at various strengths of Bose-Fermi repulsion. Then we obtain analytical descriptions of the density profiles in the regimes of weak interaction and phase separation and, hence, obtain insight into the formation and structure of the Bose-Fermi interface. We also discuss the weak finite-temperature effects on the Bose-Fermi overlap.

As an elementary example of dynamic behavior, the RBM of a BEC immersed in a DFG is theoretically studied in the current work. We consider the condition of our experiments [27] on the RBM, and the dynamics of the DFG is investigated in three ways. In the first case, we assume that the DFG adiabatically follows the oscillation of the BEC. Our second approach considers single fermion trajectories in the full phase-separation limit (PSL). Finally, we also perform numerical simulations for fermions using the test-particle method (TPM). Our results show that, when the Bose-Fermi s-wave scattering length a_{bf} increases from 0, the RBM frequency ω remains almost constant until the fermions are depleted from the trap center by the BEC. Then the frequency increases dramatically across the phase separation until it levels off at the full PSL. The relation between the plateau value of ω and the number ratio N_b/N_f unveils the essential role of the compressional character of the breathing mode.

In Sec. II, we first present our mean-field model, which has been used in Refs. [26,27], and study the static properties of a Bose-Fermi mixture with tunable repulsive interspecies interaction. Then we obtain analytical results for the situations of weak interaction and phase separation and, in particular, intuitively explain the structure of the interface in immiscible Bose-Fermi mixtures. In Sec. III, we develop three models to study the radial breathing mode of a BEC immersed in a large Fermi sea, and the frequency of the RBM at different strengths of repulsion is calculated. We compare our results from different models and discuss the validity of the adiabatic Fermi sea (AFS) approximation. In Sec. IV, we summarize our results and their impacts.

II. STATIC PROPERTIES

In our recent work [26,27], we developed a numerical mean-field model to calculate static density profiles of Bose-Fermi mixtures at zero temperature. At finite temperatures, we use the density of the BEC and fermions to calculate the mean-field potential and estimate the thermal-boson density. Here we first describe this model in detail; the basic ideas are mentioned in the Supplemental Material to Ref. [26]. Then we calculate the Bose-Fermi overlap Ω, which is an experimental observable. We further obtain analytical results for Ω at weak interaction and full phase separation. Finally, finite-temperature effects on densities are estimated.

A. Numerical model

We start with the zero-temperature energy functional of the mixture, which is [28]

$$E = \int d^3r \left[-\frac{\hbar^2}{2m_b}\psi^*\nabla^2\psi + V_b\psi^*\psi + \frac{1}{2}g_{bb}(\psi^*\psi)^2 \right.$$
$$+ \frac{1}{9}\frac{\hbar^2}{2m_f}(\nabla\sqrt{n_f})^2 + V_f n_f + \frac{\hbar^2}{2m_f}\frac{3}{5}(6\pi^2)^{2/3}n_f^{5/3}$$
$$\left. + g_{bf}n_b n_f \right]. \tag{1}$$

Here ψ is the order parameter of the BEC, n_f is the number density of the fermions, V_b and V_f are the corresponding trapping potentials, and $g_{bb} = 4\pi\hbar^2 a_{bb}/m_b$ and $g_{bf} = 2\pi\hbar^2 a_{bf}(m_b^{-1} + m_f^{-1})$ are the boson-boson and boson-fermion coupling constants. Considering the static case, we ignore the dynamic phase of ψ and have $\psi = \psi^* = \sqrt{n_b}$, where n_b is the BEC number density. Consequently we can replace $-\psi^*\nabla^2\psi$ in Eq. (1) with $(\nabla\sqrt{n_b})^2$. The term with ∇ for bosons arises from the kinetic energy and can be ignored in the Thomas-Fermi (TF) limit. The ∇ term for fermions is the leading term from the density-gradient correction, which is much smaller than the other terms under the relevant experimental conditions [26].

In order to obtain the static solution, we minimize the energy functional with the steepest descent method [also known as the imaginary time evolution] [29]. The evolution of the densities from step j to step $j + 1$ follows

$$\sqrt{n}_{j+1} = \sqrt{n}_j - \frac{\delta E}{\delta n}\sqrt{n}_j\Delta\tau, \tag{2}$$

where $\Delta\tau$ is the step size of the evolution, and its value should be large enough to ensure fast convergence but small enough to avoid numerical instability. We normalize atom numbers after each time step under the constraints

$$N_b = \int n_b d^3r,$$
$$N_f = \int n_f d^3r. \tag{3}$$

The equilibrium solution of n_b and n_f is obtained when the algorithm converges.

The zero-temperature density profiles at $a_{bf} = 0$, $300a_0$, and $600a_0$ are plotted in Fig. 1 for our typical experimental conditions [26] with $N_b = 1.5 \times 10^4$ bosons and $N_f = 1.5 \times 10^5$ fermions. The radial center-of-mass trapping frequency is 171 Hz (300 Hz) for bosons (fermions), and the aspect ratio of the elongated trap is 7.55. We observe that the fermions are depleted from the trap center by the increasing a_{bf} to a moderate value, slightly above $300a_0$. With stronger repulsions, the BEC is further squeezed to form a core that is surrounded by the fermions via a thin interface.

B. Overlap function

We consider the normalized boson-boson-fermion (BBF) overlap at zero temperature, because three-body recombination losses are dominated by BBF collisions and they can be used to probe the interface [26]. We ignore other three-body
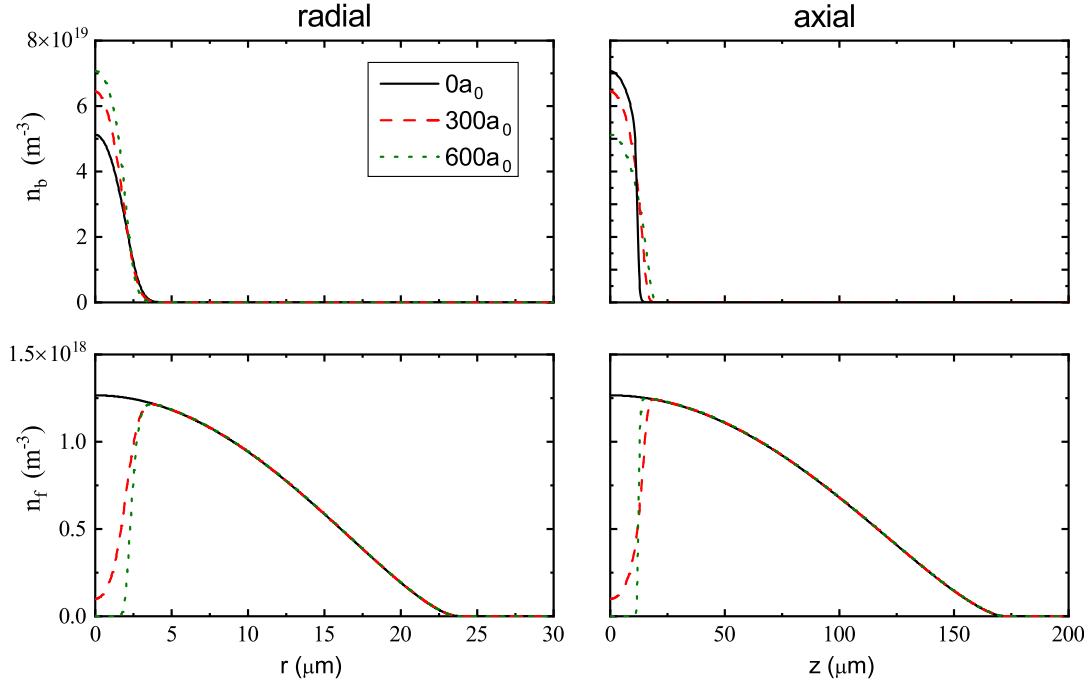
FIG. 1. Density profiles of the BEC (n_b) and the fermions (n_f) along the radial (r; left column) and the axial (z; right column) axes. The solid black, dashed red, and dotted green curves are calculated for a_{bf} values of 0, $300a_0$, and $600a_0$, respectively.

collisions involving two or more identical fermions, because they are suppressed at low temperatures by Pauli blocking. Three-boson recombination is also negligible under the relevant experimental conditions, as the boson-boson scattering length is very small. The normalized BBF overlap is

$$\Omega = \frac{\int n_b^2 n_f dV}{\int \tilde{n}_b^2 \tilde{n}_f dV}, \qquad (4)$$

where $\tilde{n}$ denotes the density profile in the absence of Bose-Fermi interaction. The overlap function from the numerical results is plotted as the solid black line (TF + B + F) in Fig. 2. We observe a smooth decrease in Ω as a_{bf} increases.

Now we compare our full model with the TF limit to study the influence from the kinetic energy of the BEC and the density gradient of the fermions. Within the TF approximation, we remove $\nabla\sqrt{n_b}$ and $\nabla\sqrt{n_f}$ in Eq. (1) and obtain Ω. The results are plotted as the dotted black line (TF) in Fig. 2. We observe that the overlap decreases drastically and vanishes near $a_{bf} = 600a_0$, where phase separation takes place.

We further test the importance of $\nabla\sqrt{n_f}$ by excluding it from the full model while keeping the BEC kinetic energy term. The results are shown as the dashed black curve (TF + B) in Fig. 2. We find the TF + B curve to be very close to the full calculation, indicating the fact that the influence from the fermion density gradient is very weak.

C. Analytical results at small a_{bf}

We start from the mean-field TF density profiles in a harmonic trap as

$$n_f = n_{f0}\left(1 - \frac{g_{bf}n_b}{\mu_{f0}}\right)^{3/2}, \qquad (5)$$

$$n_b = n_{b0}\left(1 - \frac{U_b + g_{bf}n_f}{\mu_{b0}}\right), \qquad (6)$$

where n_{f0} and n_{b0} are the peak densities of the fermions and the bosons, μ_{f0} and μ_{b0} the global (position independent) chemical potentials, and U_b the trapping potential of bosons. In Eq. (5), we have applied the fermionic reservoir approximation [26] by ignoring any trapping potential U_f for fermions and treat the fermions as a Fermi sea with a constant chemical potential. The fermionic reservoir approximation is valid as long as the BEC extends over a region much smaller than the fermion gas.
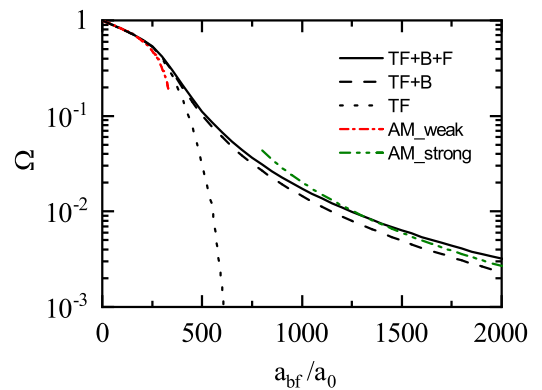

FIG. 2. Comparison between the Ω from the numerical algorithms and the Ω from the analytical models. The full numerical model produces the solid black curve (TF + B + T), application of the TF approximation for both components in the numerical model gives the dotted black line (TF), and use of the TF approximation only for the fermions leads to the dashed black curve (TF + B). The results from the analytical models for weak (AM_weak; dash-dotted red curve) and strong (AM_strong; dash-dot-dotted green curve) repulsive interactions are compared to the numerical results.

We first consider the homogeneous case, where U_b vanishes. In the weak-interaction regime, we perform a Taylor expansion in g_{bf} and find $\delta\mu_b/\delta n_b \approx g_{bb} + g_2$, where

$$g_2 = -\frac{3}{2}g_{bf}^2\frac{n_f}{\mu_f}, \tag{7}$$

and for the leading term we have $n_f \approx n_{f0}$ and $\mu_f \approx \mu_{f0}$. This correction, g_2 to g_{bb}, indicates a fermion-mediated boson-boson interaction, which has been observed in Refs. [25,30] and interpreted as the long-wavelength limit of the Ruderman-Kittel-Kasuya-Yosida [31] interaction. In our Eq. (7) the scaling $g_2 \propto g_{bf}^2$ means that the mediated interaction is a second-order mean-field effect in the adiabatic limit.

Now we consider trapped mixtures and the effects of a small a_{bf} to the overlap factor Ω. In this case, the fermions are slightly repelled from the trap center while the BEC is weakly compressed. Then the Taylor expansion of Ω on the small parameter $\eta = g_{bf}n_{b0}/\mu_{f0}$ leads to

$$\Omega = 1 - \eta + \left(\frac{2}{11} + \frac{9d}{10}\right)\eta^2 + \left(\frac{10}{429} - 2d\right)\eta^3 + O[\eta^4], \tag{8}$$

where $d = \mu_{f0}n_{f0}/\mu_{b0}n_{b0}$ is of the order of 1 under our experimental conditions. Because within the TF description the overlap function does not depend on the aspect ratio of the trap, we evaluate Eq. (8) up to third order and plot the result in Fig. 2 as the dash-dotted red curve. This analytical model agrees very well with the numerics in the weak-interaction regime, and it only begins to deviate near the region of phase separation.

D. The analytical model at large a_{bf}

Let us discuss the opposite limit, where the a_{bf} is very large and the fermions and bosons are separated. Obviously, the residual overlap in this regime is beyond the TF approximation, and we have to consider at least the kinetic energy of the BEC. We start from an infinite system without a trapping potential, where we have only the BEC (fermions) at $x \to \infty$ ($x \to -\infty$) and the components are separated by an interface parallel to the y-z plane.

By applying the TF approximation to fermions and the pressure balance at the interface (see Appendix B), we obtain the dimensionless differential equation for the order parameter $\psi = \sqrt{n_b}$ of the BEC as

$$\phi = -\frac{\partial^2\phi}{\partial X^2} + \phi^3 + \frac{5\eta}{4}(1 - \phi^2\eta)^{3/2}\phi, \tag{9}$$

where ψ is normalized by $\phi = \psi/\sqrt{\mu_{b0}/g_{bb}}$, and x by the BEC healing length $\xi_{b0} = \hbar/\sqrt{2m_b\mu_{b0}}$ as $X = x/\xi_{b0}$. The solution with boundary condition $\phi(+\infty) = 1$ and $\phi(-\infty) = 0$ is given by

$$\frac{dX}{d\phi} = \sqrt{\frac{2}{(1-\phi^2)^2 - (1-\phi^2\eta)^{5/2}\Theta(1-\phi\sqrt{\eta})}}, \tag{10}$$

where Θ is the Heaviside step function. The one-dimensional BBF integral along the x axis is then

$$\begin{aligned} I_x &= \frac{1}{2}\int_{-\infty}^{+\infty} n_b^2 n_f \, dx \\ &= \frac{\sqrt{2}\xi_b}{2}n_{b0}^2 n_{f0}\eta^{-5/2} \\ &\quad \times \int_0^1 du \frac{u^4(1-u^2)^{3/2}}{\sqrt{(1-u^2/\eta)^2 - (1-u^2)^{5/2}}}, \end{aligned} \tag{11}$$

where we have used $u = \phi\sqrt{\eta}$ for simplification and the factor $1/2$ results from the suppression of thermal bunching in a BEC involving two identical bosons [see also Eq. (13)]. We recognize that the overlap integral decreases proportionally to $a_{bf}^{-5/2}$ at strong repulsive interactions.

To calculate Ω for a trapped mixture in the phase-separated regime, we consider that ξ_b is much smaller than R_b and R_f. Then the atom number conservation and the pressure balance at the interface fix the equilibrium condition of the system, e.g., R_b, R_f, and the radial position of the interface $r = \zeta$ (see Appendix B). We evaluate I_x at the interface and multiply it by the surface of the ellipsoidal interface, whose semiaxes are $(\zeta, \zeta, A\zeta)$. We then normalize the outcome with the overlap integral at zero a_{bf}, which is obtained from the numerical model (TF + B), while an analytical approximation is also available [26]. The resulting Ω is plotted in Fig. 2 as the dash-dot-dotted green curve, which is consistent with the numerical model. The small discrepancy between the numerical and the analytical results is probably caused by the surface tension of the interface [32] and the finite value of ξ_b/R_b and ξ_b/R_f.

We also compare this result with a simple intuitive model, which assumes that the BEC is facing a hard wall at the interface and its $n_b(x) = n_{b0}\tanh^2(x/\sqrt{2}\xi_{b0})$ is suppressed to 0 within its healing length ξ_b. At the steep and rigid mean-field potential induced by the BEC, the Fermi sea is filled up to the Fermi energy. The corresponding I_x agrees with the full calculation with a deviation of less than 20% when $\eta \gg 1$.

E. The thermal faction of bosons

In this model we assume n_t to be influenced by n_b and n_f, but not vice versa. This approximation is valid as long as we have $n_t \ll n_b$. We then calculate $n_t(r, z)$ with a Bose-Einstein distribution for thermal bosons, which is

$$n_t = \left(\frac{m_b k_B T}{2\pi\hbar^2}\right)^{3/2}\mathrm{Li}_{3/2}[e^{(\mu-U_b)/k_B T}], \tag{12}$$

where the total effective potential U_b for a thermal boson is $V_b + 2g_{bb}n_b + g_{bf}n_f$ and $\mathrm{Li}_{3/2}$ is the polylogarithm function of order $3/2$. The chemical potential μ_b of the BEC is obtained from the known n_b and n_f using $\mu_b\psi = (-\hbar^2\nabla^2/2m_b + g_{bb}n_b + g_{bf}n_f)\psi$ and $\psi = \sqrt{n_b}$. The temperature T is fixed numerically to fulfill the atom number constraint $N_t = \int n_t dV$, and we finally get the density distribution n_t, which is shown in Fig. 3. Here the total boson number is 3×10^4 and the BEC fraction is 50%. We note that the thermal bosons form a shell-like structure at the edge of the BEC, because both the BEC and the fermions are repulsive to thermal bosons.
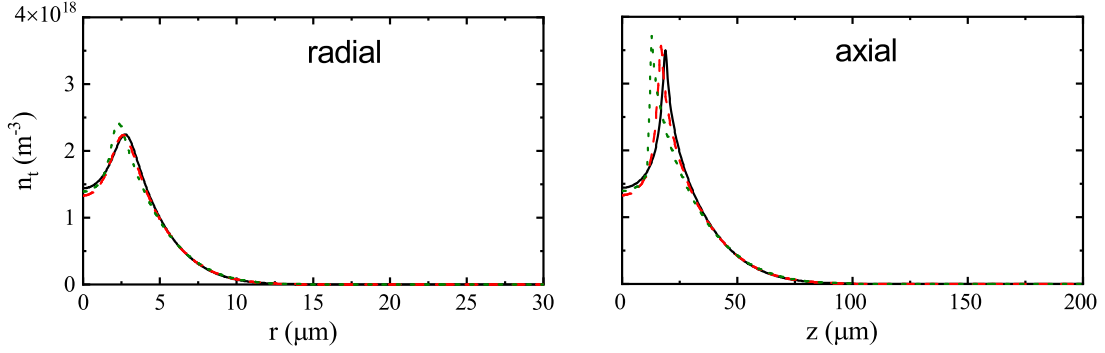
FIG. 3. Density profiles of the thermal bosons (n_t) along the radial (r; left column) and the axial (z; right column) axes. The solid black, dashed red, and dotted green curves are calculated for a_{bf} values of $0a_0$, $300a_0$, and $600a_0$, respectively. We have used the n_b and n_f from Fig. 1 to calculate the mean field for thermal bosons.

Although the density n_t of the thermal component of the boson gas is typically almost two orders of magnitude lower than the BEC density n_b, the significant thermal fraction (up to $\sim$50%) of the bosons under typical experimental conditions leads to a correction to the total overlap between bosons and fermions. The generalized overlap Ω including the thermal bosons is defined as [26]

$$\Omega = \frac{\int \left(\frac{1}{2}n_b^2 n_f + n_b n_t n_f + n_t^2 n_f\right) dV}{\int \left(\frac{1}{2}\tilde{n}_b^2 \tilde{n}_f + \tilde{n}_b \tilde{n}_t \tilde{n}_f + \tilde{n}_t^2 \tilde{n}_f\right) dV}, \qquad (13)$$

where n_t and $\tilde{n}_t$ are the thermal boson density with and without the Bose-Fermi interaction.

We calculate Ω from n_b, n_f, and n_t and plot the results as the dashed green curve in Fig. 4. The solid black curve in Fig. 4 excludes thermal bosons and is identical to the one in Fig. 2. If we ignore the interaction between the thermal bosons and the fermions, Ω values become the dotted red curve in Fig. 4. We find that the residual of Ω in the strong-interaction regime has a value of a few percent, and it slowly decreases when the repulsion between the thermal bosons and the fermions is considered.
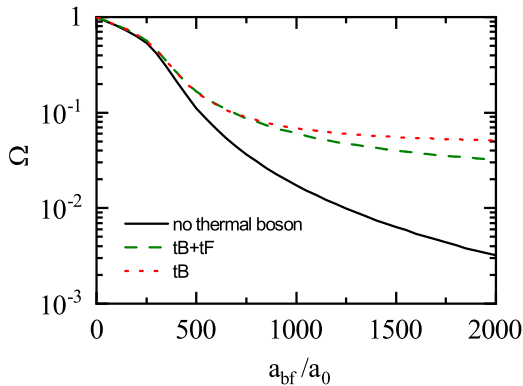

FIG. 4. Comparison of the overlap factors Ω from the numerical model with vs without thermal bosons included. The solid black line is identical to the one in Fig. 2, which ignores the thermal bosons. The dashed green and dotted red curves show the results including thermal bosons, which are interacting either with both the BEC and the fermions (tB + tF) or with only the BEC (tB).

F. Finite-temperature effects on fermions

At a finite temperature the BEC is only weakly influenced by the thermal bosons, therefore we can analyze the degenerate and nondegenerate parts separately. But we cannot define a thermal or degenerate part of the fermionic gas since all the single-particle orbitals are correlated. Consequently we estimate the finite-temperature effects of fermions in a perturbative way, i.e., by calculating the finite-T fermion density n_f from the n_b known at zero T with a Fermi-Dirac distribution. We discuss only the temperature effects on the overlap integral, i.e., the numerator in Eq. (13), because the denominator is fixed in our definition of generalized Ω.

With a typical temperature of $T/T_f \approx 0.12$, n_f is about 5% lower than the zero-T solution at the trap center and lightly spreads out at the edge, e.g., $r = R_f$ in the radial direction. Since our experiments have $R_f/R_b \approx 8$, we ignore the inhomogeneity of n_f in the BEC region and expect an approximately 5% downshift of the overlap integral. On the other hand, the thermal boson cloud extends much wider than the BEC and is much less sensitive to the finite-T correction of n_f.

Another effect, which also exists at zero temperature, is the unitary limit of the cross section of the Bose-Fermi scattering. The fermions have a kinetic energy of the order of the Fermi energy E_F, which is much higher than the kinetic energy of the bosons and leads to a reduction in the Bose-Fermi cross section. Under the relevant experimental conditions we have $1/k_F \approx 4500a_0$, where $E_F = \hbar^2 k_F^2/2m_f$. Since the mean kinetic energy of fermions at the trap center is $3E_F/5$, we estimate that the cross section scales proportionally to $a^2/(1 + 0.6 \times a^2 k_F^2)$. Therefore the reduction in the Bose-Fermi cross section is negligible under typical experimental conditions, where a_{bf} is always below about $2000a_0$.

III. RADIAL BREATHING MODE

In our recent experiment on an elongated Bose-Fermi mixture [27], we have observed a significant frequency shift of the RBM of the BEC when phase separation takes place. This motivates us to theoretically investigate the collective mode of a BEC immersed in a large Fermi sea at various values of a_{bf}. To model the dynamics of the BEC, we use the GPE and include a mean-field potential, $g_{bf}n_f$, formed by the fermions.

For the dynamics of fermions, we utilize different models. The first model we introduce here is the adiabatic Fermi sea model, which assumes that the fermions adapt adiabatically to the perturbations of the BEC. This model can be solved by either performing time evolutions (TEs) or extracting eigenvalues (EGs) from linearized equations. Then in the second model, we use the collisionless Boltzmann-Vlasov equation (BVE) to describe the fermions. The BVE is solved numerically with the test-particle method, while an analytical result is also achieved at the phase-separation limit. We obtain the RBM frequency ω from different models and compare the results.

In our following calculations we approximate our elongated mixture to an axially invariant system with cylindrical symmetry. The radial plane of the model corresponds to the radial plane of the mixture at the trap center. The static density profiles of the mixture in the radial plane are obtained from the numerical model described in Sec. II A. The temperature of the system is assumed to be 0 in our oscillation models.

A. Adiabatic Fermi sea approximation

If the density of fermions is high enough to support a Fermi velocity $v_F = \sqrt{2E_F/m_f}$ much higher than the sound velocity $v_s = \sqrt{g_{bb}n_b/m_b}$ of the BEC, the fermions follow adiabatically the fluctuations of the BEC density within a mean-field picture [16]. This AFS approximation is valid under relevant experimental conditions as long as the fermions are not depleted from the BEC region.

We formally write down the TE equation of the BEC dressed by the adiabatic Fermi sea as

$$i\hbar\frac{\partial\psi}{\partial t} = -\left[\frac{\hbar^2}{2m_b}\nabla^2 + V_b + g_{bb}|\psi|^2 + g_{bf}n_f\right]\psi. \quad (14)$$

The time-dependent fermion density $n_f = C_f(\mu_{f0} - g_{bf}|\psi|^2)^{3/2}\Theta(\mu_{f0} - g_{bf}|\psi|^2)$, where μ_{f0} is the global Fermi energy and $C_f = (2m_f/\hbar^2)^{3/2}/6\pi^2$, is calculated with the TF approximation and fermionic reservoir approximation of the fermions.

In order to numerically solve Eq. (14), we approximate our cigar-shaped cloud with a cylindrical system, whose radial plane represents the radial plane of the mixture at the trap center. We describe ψ in the radial plane by setting up a one-dimensional complex-valued grid for ψ along the radial direction.

Our first way to solve Eq. (14) is by numerically calculating the time evolution of ψ. Inspired by our experiment [27], where we excited the RBM by switching a_{bf} between a small and a large value, we perform a similar process in our simulations for a given a_{bf}. We take the static solution ψ_0 at $a_{bf} - 100a_0$ as the initial value of ψ. Then we switch to a_{bf} and let ψ evolve in time according to Eq. (14), while the TF density n_f at each time step is calculated from $|\psi|^2$ at that moment. We record the averaged BEC width $\langle r \rangle = \int dr\, r W(r)/\int dr\, W(r)$, where the weight function is $W(r) = 2\pi r n(r)$, as a function of time and fit it to a cosine function to extract the oscillation frequency ω.

The calculated dependence of ω on the interaction strength is plotted as solid curves in Fig. 5 and labeled AFS-TE for the AFS approximation and the time-evolution method. The solid black curve corresponds to an experimental setting with
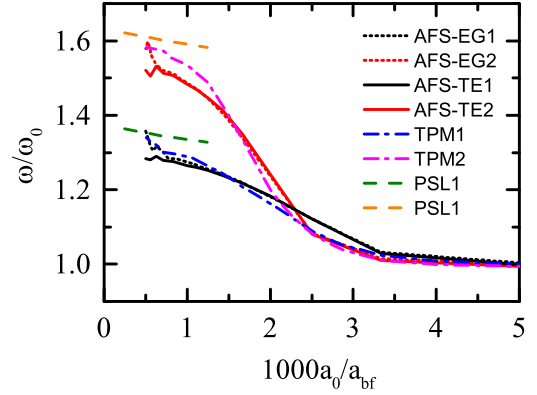

FIG. 5. Radial breathing mode frequency shift ω/ω_0 calculated from different models and parameters. Two sets of atom numbers are used here: Set 1, with $N_b = 1.6 \times 10^4$ and $N_f = 1.03 \times 10^5$; and Set 2, with $N_b = 8 \times 10^3$ and $N_f = 1.68 \times 10^5$. The solid black (red) curve represents the AFS approximation obtained by the direct time evolution (AFS-TE) method for Set 1 (Set 2). The dotted black (red) curve also includes the AFS approximation but is obtained by finding the eigenvalues of the linearized equations (AFS-EG) for Set 1 (Set 2). The blue and pink dash-dotted curves show the results of the GPE-BVE mode solved by the TPM for two sets of parameters. The outcomes of the PSL model at large a_{bf} values are shown by the dashed green and orange curves for the two sets.

a boson number of $N_b = 1.6 \times 10^4$ and a fermion number of $N_f = 1.03 \times 10^5$ (called Set 1), while the solid red curve uses $N_b = 8 \times 10^3$ and $N_f = 1.68 \times 10^5$ (Set 2). These parameters correspond to our experimental conditions [27]. We use $x = 1000a_0/a_{bf}$ for the horizontal axis in the plot, and the y axis is normalized to the RBM frequency ω_0 at $a_{bf} = 0$. The AFS-TE model shows that the RBM frequency ω barely changes at small scattering lengths. Then it starts to increase rapidly near $x = 3$, where the fermions are depleted from the trap center. Finally, ω tends to reach a maximum frequency shift near around $x = 1$. The numerics begin to fail when the mixture is deeply in the phase-separation regime and the interface depth is comparable to the grid step size.

We note that the maximum shift of ω is higher when N_f/N_b is larger. So we define the boson number fraction $Q = N_b/(N_b + N_f)$, fix the total atom number $N_b + N_f = 1.5 \times 10^5$, and calculate the RBM frequency at $a_{bf} = 1300a_0$ for various Q values. The results are presented as the black curves in Fig. 6 for a range of Q that is reachable in the experiment. We find that ω/ω_0 increases more rapidly when Q is close to 0.

As an alternative numerical method, we linearize and solve Eq. (14) for a small perturbation $\delta\psi$ and $\delta n_f = -(3/2)g_{bf}C_f^{2/3}n_f^{1/3}\delta(\psi^*\psi)$. We take the ansatz $\psi = (\psi_0 + ue^{-i\omega t} + v^*e^{i\omega t})e^{-i\mu_b t/\hbar}$ near the equilibrium solution $\psi_0 = \psi_0^* = \sqrt{n_b}$ and arrive at the linearized effective GPE as

$$\begin{aligned} \hbar\omega u &= [H_b + (2g_{bb} + g_2)n_b]u + (g_{bb} + g_2)n_b v, \\ -\hbar\omega v &= [H_b + (2g_{bb} + g_2)n_b]v + (g_{bb} + g_2)n_b u, \end{aligned} \quad (15)$$

where $H_b = -(\hbar^2/2m_b)\nabla^2 + V_b + g_{bf}n_f - \mu_b$ accounts for the kinetic energy, the boson trapping potential, the mean-field potential induced by a static Fermi sea, and the global
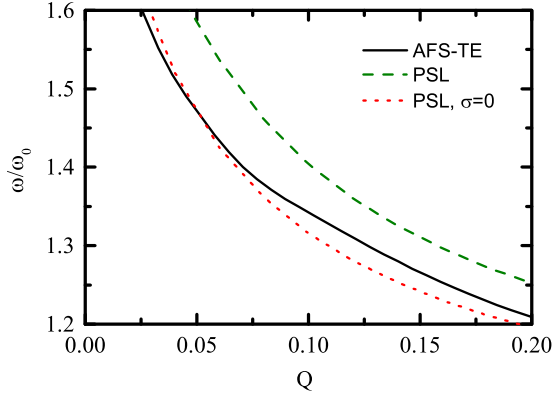
FIG. 6. RBM frequency ω/ω_0 at the PSL as a function of the boson number fraction $Q = N_b/(N_b + N_f)$. The solid black curve is calculated from the AFS-TE model. The PSL model with and without ($\sigma = 0$) the surface tension effects gives the dashed green and dotted red curves, respectively. We use a total atom number of 1.5×10^4 and $a_{bf} = 1300a_0$.

chemical potential μ_b of the BEC obtained from the static solution. The boson-boson interaction that is mediated by the Fermi sea is given in Eq. (7).

In order to numerically solve Eq. (15) for a cylindrical system, we discretize $u(r)$ and $v(r)$ along the radial direction. With the n_b and n_f obtained in Sec. II A, we obtain the eigenfrequency ω by diagonalizing Eq. (15) in its matrix form with a regularized boundary condition. The calculated ω/ω_0 values of the lowest RBM are shown in Fig. 5 as the black and red dotted curves (AFS-EG1 and AFS-EG2) for the two sets of atom numbers. Although the diagonalization method requires $n_f > 0$ and becomes no longer fully valid when a_{bf} is so large that fermions are depleted from the trap center, we find that its results agree very well with the outcomes of the direct time evolution before numerical instabilities take over in the deeply phase-separated regime.

Finally, we discuss our Eq. (15) in comparison with other experimental [25] and theoretical (e.g., [33–35]) works on weakly interacting Bose-Fermi mixtures. In the earlier works, a simple replacement of the boson coupling constant $g_{bb} \rightarrow g_{bb} + g_2$ transforms the dynamics from a pure BEC to a weakly interacting Bose-Fermi mixture. In our model, such a transformation is not explicit in Eq. (15) because of the terms proportional to $2g_{bb} + g_2$. Our results recover $g_{bb} \rightarrow g_{bb} + g_2$ only if we take the limit of $g_{bf}n_b \ll \mu_f$, where $g_{bf}\delta n_f \approx g_2 n_b$ is valid. Moreover, we find that a small g_{bf} also induces a correction (buoyancylike effect) $-\frac{3n_f V_f}{2\mu_f V_b} g_{bf}$ to the boson potential V_b when a weak fermion potential $V_f \ll \mu_f$ is considered. In general, we expect our results to be valid also beyond the weak-interaction regime.

B. Kinetic equation simulation for fermions

To describe the dynamics of the degenerate single-component Fermi gas by first principles, we utilize the BVE with vanishing collisions, i.e.,

$$\partial_t f + \frac{1}{m_f}\vec{p} \cdot \vec{\nabla}_r f - \frac{1}{m_f}\vec{F}_f \cdot \vec{\nabla}_v f = 0, \qquad (16)$$

where $f(\vec{p}, \vec{r})$ is the fermion distribution function in the phase space, and m_f the mass of a single fermion. The force $\vec{F}_f(r, t) = -\partial[V_f(r) + g_{bf}n_b(r, t)]/\partial r$ on the fermions is given by the trapping potential $V_f(r) = m_f \omega_f^2 r^2/2$ and the mean-field repulsion $g_{bf}n_b$ from the BEC.

Equation (16) can be solved numerically with the quasi-particle method [14,20], which uses a cloud of $\tilde{N}$ classical pseudoparticles (test particles) with mass m_f to sample the phase space of N real fermions. We initialize the $(\vec{r}, \vec{p})$ values of paritest particles according to the Fermi-Dirac distribution at zero temperature. The kinetic equation is then simulated with the Newtonian equations $\dot{\vec{p}} = \vec{F}_f(r, t)$ and $\dot{\vec{r}} = \vec{p}/m_f$ of the test particles. The real fermion density $n_f(\vec{r})$ is calculated from the number of test particles in the interval $(r, r + dr)$ and scaled by a factor of $N/\tilde{N}$.

In our calculations for a cylindrical system, we implement a one-dimensional spatial grid for ψ. The finite value of $\tilde{N}$ induces statistical noises of n_f, which depends also on the size dr of the grid. This statistical noise is similar to finite-temperature effects, and we take values of $\tilde{N}$ corresponding to $T/T_F \lesssim 0.1$. In order to excite the collective mode, we start with the static densities at $a_{bf} = 0$ and apply three consecutive quenches of the scattering length a_{bf} between 0 and $700a_0$, which closely imitates the relevant experimental sequence [27]. After the excitation stage, the time evolutions of the effective width $\langle r \rangle$ for the BEC and the fermions are recorded to extract the frequency.

The typical time evolutions of the $\langle r \rangle$ of the BEC (solid blue curve) and the fermions (dotted red curve) are plotted in Fig. 7. Our calculation uses atom numbers from Set 1 (see Sec. III A). And $a_{bf} = 100a_0$ and $a_{bf} = 1000a_0$ apply to Figs. 7(a) and 7(b), respectively. We recognize that the oscillation is not necessarily a simple sinusoidal wave, and it contains possibly multiple frequency components. So we apply the fast Fourier transformation to the data and obtain the power spectra, which are shown in Fig. 8.

We find that two frequency components are important in the spectra; one is close to or slightly above $\omega/\omega_0 = 1$ and the other is close to $\omega/\omega_0 = 1.8$. Keep in mind that $\omega_f/\omega_b = 1.75$ and the BEC extends much more narrowly than the fermionic gas; we recognize the higher-frequency component as the single-fermion mode, which is only slightly changed by the small BEC. On the other hand, the main peak in the BEC spectrum indicates that the BEC RBM is coupled to the fermions and forms a lower branch of the oscillating spectrum.

To be consistent with the analysis of frequencies in our experimental work [27], we fit the oscillation of the width with a cosine function and extract the frequency ω. The results are plotted in Fig. 5. The blue (pink) dash-dotted line shows the results for Set 1 (Set 2). The results from the TPM are consistent with the AFS model. Furthermore, we also vary the initial excitations, e.g., the amplitude of the oscillation, and extract ω in different time sections of the evolution. And we observe only minor changes (less than about 5%) of the value of ω. Finally, although our test-particle method is a zero-T model, the statistical noise in n_f is similar to the thermal noise. So our results suggest qualitatively that the temperature does not have significant influence on the RBM frequency under the conditions for relevant experiments.
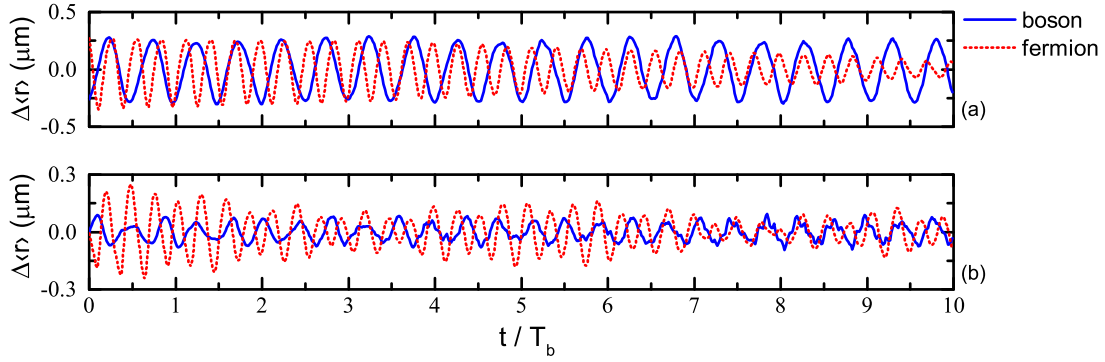
FIG. 7. Simulated width evolution of the bosonic (solid blue curve) and the fermionic (dotted red curve) clouds, where the GPE-BVE model is used. The time t is normalized to the single-boson COM period T_b in the trap. The y axis shows the deviation of the density-averaged width $\langle r \rangle$ of the cloud from its mean value. The oscillation is excited with three consecutive quenches of the Bose-Fermi interaction (scheme Exct1). Oscillation at (a) $a_{bf} = 100a_0$ and (b) $a_{bf} = 1000a_0$.

C. Analytical model of oscillation at the phase-separation limit

At the PSL, both the static and the dynamic properties of the Bose-Fermi mixture can be studied analytically [19,32]. Following the procedure introduced in Ref. [19] for a spherical case, we investigate the RBM of the BEC in an infinitely long cylindrical mixture, which is more relevant to experiments. Starting from the TF approximation for both components, we assume that the two components in the mixture are connected by an infinitely thin interface layer, which has a surface tension effect with coefficient σ [32] (see also Appendix A). We first obtain separately the formal solution of the BEC density and the fermion phase-space distribution function $f(r, p)$, then solve the problem of the mixture by matching the boundary conditions, i.e., flux and pressure, at the interface. The equilibrium solution of the densities in the mixture is used in Sec. II D and discussed in detail in Appendix B. We now find the oscillation frequency ω of the RBM in the mixture.

The collective modes of a trapped BEC in the TF limit are well understood [9]. The radial mode of a BEC with zero angular momentum in a cylindrical system corresponds to a
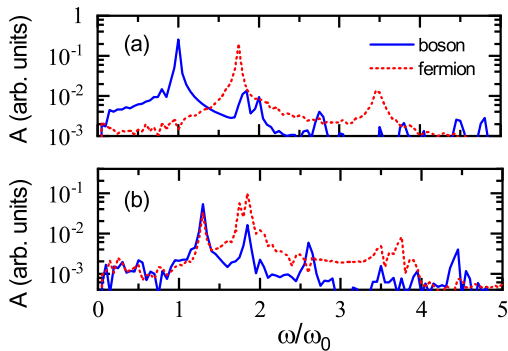

FIG. 8. FFT spectrum amplitude A of the oscillations shown in Fig. 7. The radial breathing mode frequency ω is normalized to its reference value ω_0 at $a_{bf} = 0a_0$. Results with (a) $a_{bf} = 100a_0$ and (b) $a_{bf} = 1000a_0$.

density fluctuation of

$$\delta n_b(r) \propto F\left(\frac{1+\sqrt{1+2\frac{\omega^2}{\omega_b^2}}}{2}, \frac{1-\sqrt{1+2\frac{\omega^2}{\omega_b^2}}}{2}, 1, \frac{r^2}{R_b^2}\right),$$

(17)

where F is the hypergeometric function $_2F_1$, ω the frequency of the collective mode, ω_b the COM trapping frequency of bosons, and R_b the Thomas-Fermi radius of the BEC.

At the interface $r = \zeta$ of the mixture there is no exchange of components. This means that the velocity of the BEC is equal to the speed $\dot{\zeta}$ of the moving interface. Consequently we have

$$\delta\zeta = \frac{g_{bb}}{\omega^2 m_b}\partial_r \delta n_b,$$

(18)

where we denote $\partial_r n_b = \partial n_b/\partial r$ for simplicity.

In the phase-separation limit, the kinetic equation for fermions reduces to

$$\partial_t f + \vec{v} \cdot \vec{\nabla}_r f - \omega_f^2 \vec{r} \cdot \vec{\nabla}_v f = 0.$$

(19)

We then apply the ansatz describing the deformation of the Fermi surface as $f = f_0 + \delta(|\vec{p}| - p_f)u(r, \alpha, \beta)e^{-i\omega t}$, where $\alpha = \cos\phi$, with ϕ the angle between the momentum $\vec{p}$ and the position $\vec{r}$ in the radial plane, $\beta = \cos\theta$, with θ the angle between $\vec{p}$ and the longitudinal z axis, and $p_f(r) = \sqrt{2m_f\mu_f(r)}$ the local Fermi momentum. Then we get the linearized kinetic equation

$$-i\omega u + \omega_f \rho\alpha\sqrt{1-\beta^2}\partial_r u + \omega_f(1-\alpha^2)g(r, \beta)\partial_\alpha u$$
$$+ \omega_f\alpha\beta\sqrt{1-\beta^2}\frac{r}{\rho}\partial_\beta u = 0,$$

(20)

where $\rho = (R_f^2 - r^2)^{1/2}$, with R_f the Thomas-Fermi radius of fermions, and $g(r, \beta) = (\rho\sqrt{1-\beta^2})/r - r/(\rho\sqrt{1-\beta^2})$. The corresponding solution has the form

$$u(r, \chi) = \mathcal{F}[r^2(R_f^2 - r^2)(1-\alpha^2)(1-\beta^2)]e^{-i\omega\tau/2}, \quad (21)$$

where $\mathcal{F}[x]$ is an arbitrary function of x and

$$\tau(\zeta, \alpha, \beta) = \frac{\psi_0 - \arctan[2\alpha/g(\zeta, \beta)]}{\omega_f},$$

(22)

with $\psi_0 = \pi\Theta[g(r, \beta)]$. As τ characterizes the phase of the oscillating system, we recognize it as the time it takes for a single fermion with Fermi velocity v_F to depart and then return to the interface. Equation (22) is valid when $\alpha \in [0, 1]$, and beyond that we have $\tau(-\alpha, \beta, r) = -\tau(\alpha, \beta, r)$. It is also obvious that $\tau(\alpha, -\beta, r) = \tau(\alpha, \beta, r)$.

Now we consider the nonpenetration boundary condition for fermions at the interface. It requires that

$$[u(\zeta, \alpha, \beta) - u(\zeta, -\alpha, \beta)]e^{-i\omega t} = 2m_f\alpha\sqrt{1-\beta^2}\dot{\zeta}, \quad (23)$$

where $\dot{\zeta} = \partial_t\zeta = -i\omega\delta\zeta e^{-i\omega t}$ is the velocity of the phase boundary. Taking this into Eqs. (21) and (22), the fermion perturbation is solved as

$$u(\zeta, \alpha, \beta) = 2m_f\alpha\sqrt{1-\beta^2}(-i\omega\delta\zeta)(1 - e^{i\omega\tau})^{-1}. \quad (24)$$

We may formally expand $(1 - e^{i\omega\tau})^{-1} = \sum_{n=0}^{\infty} e^{in\omega\tau}$ and recognize that this solution u is constituted of a series of elementary excitations that happened at earlier times.

The condition of pressure equilibrium at the interface is $P_b - P_f = \sigma/\zeta$, where the boson pressure is $P_b = g_{bb}n_b^2/2$ and the pressure P_f of the collisionless fermions at the interface is given by the corresponding momentum flux $\Pi(r) = (1/m_f h^3)\int d^3\vec{p}\alpha^2(1-\beta^2)p^2 f(\vec{p}, r)$ in the radial direction [19]. Together with the boson boundary condition, Eq. (18), we obtain the equation for the oscillation frequency ω as

$$\frac{\partial_r F}{F} = \frac{\omega^2 m_b\left(n_b - \frac{1}{\zeta}\frac{\partial\sigma}{\partial\mu_b}\right)}{-\frac{\sigma}{\zeta^2} + \frac{1}{\zeta}\frac{\partial\sigma}{\partial\zeta} + \frac{p_f^4 C_\Pi}{(2\pi\hbar)^3} - \partial_r(P_b - P_f)}, \quad (25)$$

where $C_\Pi = 8\omega\int_0^{\pi/2} d\phi\int_0^1 d\beta(1-\beta^2)^{3/2}\cos^3\phi\cot(\omega\tau/2)$ and all values are calculated at the interface (see Appendix D for details).

Taking typical parameters from the experiments [27], we obtain ω and show the results as the dashed green and orange curves in Fig. 5 for the two sets of atom numbers. We find that the results from the PSL model are consistent with those from other models. The PSL model predicts a slow increase in ω at the PSL and gives slightly higher ω values than other models. The Q dependence of the RBM frequency shift is presented in Fig. 6 as the dashed green curve. In order to check the influence from the surface tension effects, we also calculate ω with $\sigma = 0$ and plot the outcomes as the dash-dotted red curve in Fig. 6. The PSL model without surface tension leads to a slightly lower frequency shift.

IV. CONCLUSIONS

We have thoroughly investigated the static density profiles and the radial breathing mode in an elongated degenerate Bose-Fermi mixture. The experimentally relevant conditions from [26,27], under which the BEC is much smaller than the Fermi sea, have been considered. We first presented in detail our mean-field numerical model, which explains the smoothing of the phase separation with the kinetic energy of the BEC [27]. Then we obtained analytical forms of the density profiles in the limit of weak and strong repulsion. In particular, the latter shows intuitively the structure of the interface: The BEC at the interface behaves like it is being blocked by a wall potential, and the fermions penetrate into the mean-field potential of the BEC edge to a depth determined by the chemical potential of the Fermi sea.

We have presented three zero-temperature models for the RBM of the BEC in cylindrical mixtures, for which the results are consistent. We first describe the adiabatic Fermi sea model, which explains the significant shift of the RBM frequency observed across the phase separation of the mixture [27]. Within this model, we find the fermion-mediated interaction between bosons to be an adiabatic second-order mean-field effect, which is valid also beyond the weak-interaction regime under relevant experimental conditions. For very large a_{bf} values, another full phase-separation model considering single-fermion trajectories gives results similar to those from the AFS model. Finally, we perform test-particle simulations for the RBM, and the outcomes are almost identical to those of the AFS model for a large range of repulsion strengths. The RBM frequencies obtained from our various models are consistent.

Our theories fit nicely to the observed RBM frequencies for weak and intermediate repulsions, while the observed RBM frequency shifts in the regime of full phase separation are about half the theoretical values [27]. This discrepancy is beyond the scope of our mean-field zero-T models, and it stimulates future experiments in more deeply cooled samples with further reduced imperfections, e.g., anharmonicity of the trap. Comprehensive theories including quantitative analysis of finite-T effects [36,37], quantum fluctuations, and possible hydrodynamic properties at the interface are encouraged for study of relevant experimental situations and resolution of the remaining questions.

APPENDIX A: SURFACE TENSION AT THE INTERFACE

In the phase-separation limit, the surface tension coefficient of a flat boson-fermion interface is [19,32]

$$\sigma(\kappa) = \frac{\hbar\mu_b^{3/2}}{g_{bb}\sqrt{m_b}}G(\kappa), \quad (A1)$$

where μ_b is the chemical potential of the BEC, $G(\kappa) = \int_0^1 dx\sqrt{(1-x^2)^2 - (1-x^2/\kappa^2)^{5/2}\Theta(\kappa - x)}$, and $\kappa = \sqrt{g_{bb}\mu_f/g_{bf}\mu_b}$.

Considering a mixture in a harmonic trap with boson COM frequency ω_b we have

$$\frac{\partial \sigma}{\partial \mu_b} = \frac{\sigma}{\mu_b}\left(\frac{3}{2} - \frac{\kappa G'(\kappa)}{2}\right) = \frac{\sigma}{\mu_b}C_\sigma, \tag{A2}$$

$$\frac{\partial \sigma}{\partial r} = \frac{r\sigma}{r^2 - R_b^2}\left(\frac{3}{2} - \frac{\kappa G'(\kappa)}{2}\right) = -\frac{m_b\omega_b^2}{2\mu_b}r\sigma C_\sigma, \tag{A3}$$

where G' is the derivative of the numerical function G, and $C_\sigma = 3/2 - \kappa G'(\kappa)/2$. Here we have used the fermionic reservoir approximation, which ignores the dependence of μ_f on r.

APPENDIX B: STATIC DENSITY PROFILES AT THE PSL

Within the TF approximation, the density profiles of a phase-separated Bose-Fermi mixture can be obtained analytically [19,32]. The conservation of atom numbers and the pressure balance at the interface require that

$$\frac{N_b}{A} = \frac{R_b^5(m_b\omega_b/\hbar)^2}{2a_{bb}}\left(\frac{\zeta^3}{3R_b^3} - \frac{\zeta^5}{5R_b^5}\right), \tag{B1}$$

$$\frac{N_f}{A} = \frac{R_f^6(m_f\omega_f/\hbar)^3}{72\pi}\left(\frac{3\pi}{2} - K(\zeta/R_f)\right), \tag{B2}$$

where A is the aspect ratio of the trap, N_b and N_f the boson and fermion numbers, and $K(x) = x(1 - x^2)^{1/2}(14x^2 - 3 - 8x^4) + 3\arcsin(x)$. The interface position ζ and TF radii R_b and R_f of the BEC and the fermions are all given in the radial plane.

The pressure balance at the interface is

$$P_b - P_f = c_\sigma \sigma/\zeta, \tag{B3}$$

where the pressure of the BEC is $P_b = g_{bb}n_b^2/2$ with $n_b = m_b\omega_b^2(R_b^2 - \zeta^2)/2$, and the pressure of the fermions is $P_f = (2/5)C_f\mu_f^{5/2}$ with $\mu_f = m_b\omega_b^2(R_f^2 - \zeta^2)/2$ and $C_f = (2m_f/\hbar^2)^{3/2}/6\pi^2$. The coefficient c_σ is 2 for a spherical system and 1 for a cylindrical system. Since c_σ is not a constant on the interface of an elongated system and σ/ζ is much smaller than P_b and P_f under the experimental conditions, we simply use $c_\sigma = 0$ for discussion of the overlap integral. In the PSL model of the monopole mode, we calculate for both $c_\sigma = 0$ (TF limit) and $c_\sigma = 1$ (cylindrical approximation).

Using Eqs. (B1)–(B3) and evaluating σ with Eq. (A1) at the interface, we can fix R_b, R_f, and ζ and get the density distributions at the PSL.

APPENDIX C: COLLECTIVE MODE OF THE BEC

The wave equation of the BEC is

$$\omega^2 \delta n_b + \frac{g_{bb}}{m}\vec{\nabla}\cdot(n_b\vec{\nabla}\delta n_b) = 0, \tag{C1}$$

where $n_b(r)$ is the BEC density at equilibrium and δn_b is the density fluctuation. While the solution for a cylindrical system is given in Eq. (17), the solution in a spherically symmetric trap is

$$\delta n_b(r) \propto Y_l^m r^l F(\alpha^+, \alpha^-, l + 3/2, (r/R_b)^2), \tag{C2}$$

with F the hypergeometric function $_2F_1$, Y_l^m the spherical harmonic, $2\alpha^\pm = z \pm [z^2 + 2(\omega^2/\omega_b^2 - l)]^{1/2}$, $z = l + 3/2$, and $l \in \mathbb{N}$. Here we only need the case with $m = l = 0$.

APPENDIX D: EIGENVALUE EQUATION OF THE BREATHING MODE

1. Cylindrical condition

The pressure balance at the interface with a displacement of $\delta\zeta$ is

$$\frac{\partial P_b}{\partial \mu_b}\delta\mu_b - \delta\Pi + \left(\frac{\partial P_b}{\partial \zeta} - \frac{\partial P_f}{\partial \zeta}\right)\delta\zeta$$
$$= -\frac{\sigma}{\zeta^2}\delta\zeta + \frac{\partial \sigma}{\partial \mu_b}\frac{\delta\mu_b}{\zeta} + \frac{\partial \sigma}{\partial \zeta}\frac{\delta\zeta}{\zeta}. \tag{D1}$$

From Eq. (18) we find the relation between $\delta\mu_b = g_{bb}\delta n_b$ and $\delta\zeta$ as

$$\delta n_b = \frac{F}{\partial_r F}\frac{m_b\omega^2}{g_{bb}}\delta\zeta. \tag{D2}$$

Together with other relevant replacing rules,

$$\frac{\partial P_b}{\partial \mu_b}\delta\mu_b = g_{bb}n_b\delta n_b,$$
$$\frac{\partial P_b}{\partial \zeta} = P_b\frac{-4\zeta}{R_b^2 - \zeta^2},$$
$$\frac{\partial P_f}{\partial \zeta} = P_f\frac{-5\zeta}{R_f^2 - \zeta^2}, \tag{D3}$$
$$\delta\Pi = \frac{p_F^4}{(2\pi\hbar)^3}C_\Pi\delta\zeta,$$

Eq. (D1) becomes Eq. (25). And we can further simplify Eq. (25) to have

$$\frac{F_x}{F} = \frac{R_b m_b\omega^2\left(n_b - C_\sigma\frac{\sigma}{\mu_b\zeta}\right)}{-\frac{\sigma}{\zeta^2} - C_\sigma\frac{m_b\omega_b^2\sigma}{2\mu_b} + \frac{p_F^4 C_\Pi}{(2\pi\hbar)^3} - \partial_r(P_b - P_f)}, \tag{D4}$$

where we define formally $\partial F(\alpha^+, \alpha^-, 1, x^2)/\partial x = F_x$. If we apply the adiabatic fermionic reservoir approximation ($\delta\Pi = 0$) and ignore the surface tension terms, Eq. (D4) becomes extremely simple as $\omega^2 F = xF_x$. In the limit that x approaches 0, we get approximately $\omega/\omega_b \approx c_J/(\sqrt{2}x)$, where the constant $c_J \approx 2.4048$ is the first root of the Bessel function J_0 and $x \propto (N_b/N_f^{25/24})^{1/3}$ for our harmonically trapped mixture.

2. Spherical condition

For fermions the deformation of the Fermi surface is $f = f_0 + \delta(|\vec{p}| - p_f)u(r, \chi)e^{-i\omega t}$, where $\chi = \cos\theta$, with θ the angle between $\vec{p}$ and $\vec{r}$ and $p_f(r) = \sqrt{2m_f\mu_f(r)}$ the local Fermi momentum. In the case of a spherical system, we get

$$-i\omega u + \omega_f\rho\chi\partial_r u + \omega_f(1 - \chi^2)g(r)\partial_\chi u = 0, \tag{D5}$$

where $\rho = \sqrt{R_f^2 - r^2}$ and $g(r) = \rho/r - r/\rho$. The corresponding solution has the form

$$u(r, \chi) = \mathcal{F}\left[r^2(R_f^2 - r^2)(1 - \chi^2)\right]e^{-i\omega\tau/2}, \tag{D6}$$

where $\mathcal{F}$ is an arbitrary function and

$$\tau(\zeta, \chi) = \frac{\phi_0 - \arctan[2\chi/g(\zeta)]}{\omega_f}, \tag{D7}$$

where the constant ϕ_0 is fixed by the actual physics of the system.

As τ characterizes the phase of the oscillating system, we recognize it as the time it takes for a single fermion to depart and then return to the interface in the case where $\chi \in [0, 1]$ and have $\tau(\zeta, \chi) = -\tau(\zeta, -\chi)$.

We also have to apply the nonpenetration boundary condition for fermions at $r_e = \zeta$ that

$$[u(\zeta, \chi) - u(\zeta, -\chi)]e^{-i\omega t} = 2m_f \chi \dot{\zeta}, \tag{D8}$$

where $\dot{\zeta} = \partial_t \zeta = \partial_t(\delta \zeta e^{-i\omega t})$ is the velocity of the phase boundary. Finally, the fermion perturbation is solved as

$$u(\zeta, \chi) = 2m_f \chi (-i\omega \delta \zeta)(1 - e^{i\omega \tau})^{-1}. \tag{D9}$$

The equilibrium condition of the pressure at the phase boundary involves two variables, μ_b and ζ, and it is equivalent to considering the pressure balance in the laboratory frame or in a moving frame with the surface speed $\dot{\zeta}$. We assume that the BEC evolves in a quasistatic process and the equation of state is still valid, which gives $P_b = g_{bb}n_b^2/2$, and n_b depends on the oscillation of the density via $\delta \mu_b = g_{bb}\delta n_b$ and the

variation of the surface position $\delta \zeta$. On the other hand, when $|\dot{\zeta}| \ll v_F$, the Fermi pressure fluctuation at the boundary is given by the radial momentum flux element

$$\delta \Pi_{rr}(\zeta) = \frac{1}{m_f(2\pi\hbar)^3} \int d^3 p(\chi p)^2(f - f_0), \tag{D10}$$

where $\delta f = f - f_0$ is the perturbation of the fermion distribution function. Considering only the monopole mode for a spherically symmetric system and dropping $e^{-i\omega t}$ from both sides, we have

$$\frac{\partial P_b}{\partial \mu_b}\delta \mu_b - \delta \Pi + \left(\frac{\partial P_b}{\partial \zeta} - \frac{\partial P_f}{\partial \zeta}\right)\delta \zeta$$

$$= -\frac{2\sigma}{\zeta^2}\delta \zeta + 2\frac{\partial \sigma}{\partial \mu_b}\frac{\delta \mu_b}{\zeta} + 2\frac{\partial \sigma}{\partial \zeta}\frac{\delta \zeta}{\zeta}. \tag{D11}$$

We use Eq. (D3) with $C_{\Pi}(\omega, \omega_f) = 4\pi\omega \int_0^1 d\chi \chi^3 \cot(\omega\tau/2)$. Finally, the equation for ω in the spherical case is

$$\frac{\partial_r \delta n_b}{\delta n_b} = \frac{\omega^2 m_b\left(n_b - C_\sigma \frac{2\sigma}{\mu_b \zeta}\right)}{-\frac{2\sigma}{\zeta^2} - C_\sigma \frac{m_b\omega^2\sigma}{\mu_b} + \frac{p_f^4}{(2\pi\hbar)^3}C_{\Pi} - \partial_r(P_b - P_f)}. \tag{D12}$$

[1] C. Ebner and D. Edwards, Phys. Rep. **2**, 77 (1971).

[2] W. C. Stwalley and L. H. Nosanow, Phys. Rev. Lett. **36**, 910 (1976).

[3] C. J. Pethick and H. Smith, *Bose-Einstein Condensation in Dilute Gases* (Cambridge University Press, Cambridge, 2002).

[4] L. Pitaevskii and S. Stringari, *Bose-Einstein Condensation and Superfluidity* (Oxford University Press, Oxford, 2016).

[5] C. Chin, R. Grimm, P. S. Julienne, and E. Tiesinga, Rev. Mod. Phys. **82**, 1225 (2010).

[6] A. G. Truscott, K. E. Strecker, W. I. McAlexander, G. B. Partridge, and R. G. Hulet, Science **291**, 2570 (2001).

[7] F. Schreck, L. Khaykovich, K. L. Corwin, G. Ferrari, T. Bourdel, J. Cubizolles, and C. Salomon, Phys. Rev. Lett. **87**, 080403 (2001).

[8] D. Ludwig, S. Floerchinger, S. Moroz, and C. Wetterich, Phys. Rev. A **84**, 033629 (2011).

[9] L. Pitaevskii and S. Stringari, *Bose-Einstein Condensation and Superfluidity* (Oxford University Press, 2016).

[10] G. Modugno, G. Roati, F. Riboli, F. Ferlaino, R. Brecha, and M. Inguscio, Science **297**, 2240 (2002).

[11] C. Ospelkaus, S. Ospelkaus, K. Sengstock, and K. Bongs, Phys. Rev. Lett. **96**, 020401 (2006).

[12] K. Suzuki, T. Miyakawa, and T. Suzuki, Phys. Rev. A **77**, 043629 (2008).

[13] F. M. Marchetti, C. J. M. Mathy, D. A. Huse, and M. M. Parish, Phys. Rev. B **78**, 134517 (2008).

[14] M. Brack and R. K. Bhaduri, *Semiclassical Physics* (Addison-Wesley Publishing Company, Inc., 1997).

[15] A. L. Fetter and J. D. Walecka, *Quantum Theory of Many-Particle Systems* (McGraw Hill, New York, 2003).

[16] S. K. Yip, Phys. Rev. A **64**, 023609 (2001).

[17] L. Vichi, M. Inguscio, S. Stringari, and G. M. Tino, Journal of Physics B: Atomic, Molecular and Optical Physics **31**, L899 (1998).

[18] A. Lazarides and B. Van Schaeybroeck, Phys. Rev. A **77**, 041602(R) (2008).

[19] B. Van Schaeybroeck and A. Lazarides, Phys. Rev. A **79**, 033618 (2009).

[20] T. Maruyama, H. Yabu, and T. Suzuki, Phys. Rev. A **72**, 013609 (2005).

[21] I. Ferrier-Barbut, M. Delehaye, S. Laurent, A. T. Grier, M. Pierce, B. S. Rem, F. Chevy, and C. Salomon, Science **345**, 1035 (2014).

[22] M. Delehaye, S. Laurent, I. Ferrier-Barbut, S. Jin, F. Chevy, and C. Salomon, Phys. Rev. Lett. **115**, 265303 (2015).

[23] Y.-P. Wu, X.-C. Yao, X.-P. Liu, X.-Q. Wang, Y.-X. Wang, H.-Z. Chen, Y. Deng, Y.-A. Chen, and J.-W. Pan, Phys. Rev. B **97**, 020506(R) (2018).

[24] R. Roy, A. Green, R. Bowler, and S. Gupta, Phys. Rev. Lett. **118**, 055301 (2017).

[25] B. DeSalvo, K. Patel, G. Cai, and C. Chin, Nature **568**, 61 (2019).

[26] R. S. Lous, I. Fritsche, M. Jag, F. Lehmann, E. Kirilov, B. Huang, and R. Grimm, Phys. Rev. Lett. **120**, 243403 (2018).

[27] B. Huang, I. Fritsche, R. S. Lous, C. Baroni, J. T. M. Walraven, E. Kirilov, and R. Grimm, Phys. Rev. A **99**, 041602(R) (2019).

[28] A. Imambekov, C. J. Bolech, M. Lukin, and E. Demler, Phys. Rev. A **74**, 053626 (2006).

[29] W. H. Press, S. A. Teukolsky, W. T. Vetterling, and B. P. Flannery, *Numerical Recipes 3rd Edition: The Art of Scientific Computing* (Cambridge University Press, 2007).

[30] H. Edri, B. Raz, N. Matzliah, N. Davidson, and R. Ozeri, Phys. Rev. Lett. **124**, 163401 (2020).

[31] M. A. Ruderman and C. Kittel, Phys. Rev. **96**, 99 (1954).

[32] B. Van Schaeybroeck, Phys. Rev. A **78**, 023624 (2008).

[33] T. Tsurumi and M. Wadati, J. Phys. Soc. Jpn. **69**, 97 (2000).

[34] D. H. Santamore and E. Timmermans, Phys. Rev. A **78**, 013619 (2008).

[35] S. De and I. B. Spielman, Appl. Phys. B **114**, 527 (2014).

[36] X.-J. Liu and H. Hu, Phys. Rev. A **68**, 033613 (2003).

[37] P. T. Grochowski, T. Karpiuk, M. Brewczyk, and K. Rząźewski, arXiv:1911.10582.